Experimental studies of underexpanded hot jets: free jet velocity field and jet impact on a flat plate

D. M. Davidenko, C. Chauveau*, B. Sarh*, I. Gökalp*, V. N. Avrashkov**, and C. Fabre****
**ICARE – Institut de Combustion, Aérothermique, Réactivité et Environnement, CNRS*
1C avenue de la Recherche Scientifique, 45071 Orléans, France
***MAI – Moscow Aviation Institute (Technical University),*
4 Volokolamskoe shosse, GSP-4, A-80, 125993 Moscow, Russia
****AIRBUS France, S.A.S.*
316 route de Bayonne, P.O. BOX EEDR – M0111/3, 31060 Toulouse, France

Abstract

In the context of aircraft engine safety, experimental studies of underexpanded hot-gas jets are performed to provide data on the velocity field in a free jet and characterize thermal state of a titanium plate during a hot jet impact. Particle image velocimetry is applied to measure the jet velocity field for the following ejection parameters: total pressure from 2.6 MPa to 3.8 MPa, total temperature from 1770 K to 2140 K. Infrared temperature measurement are made on the back of titanium plates for the following ejection parameters: total pressure of 3.5 MPa, total temperature of 1930 K and 2080 K.

1. Introduction

The context of the present study is the survivability of the wing-engine propulsion system of aircraft exposed to engine fire. Actual international regulations for aircraft safety require that the engine frame must sustain a hot-gas impact during three minutes. The demonstration of these capability for aircraft safety certification requires both experimental and computational effort. In this context, a joint study between AIRBUS–France, ICARE-CNRS, and MAI has been conducted.

A hot-gas generator has been developed and tested at MAI providing the required range of flow parameters in the jet of combustion products (total pressure up to 4 MPa and total temperature up to 2200 K). ICARE-CNRS participated in two test campaigns providing experimental equipment for velocity and temperature measurements. In the first campaign, the velocity field of the free jet was studied using the particle image velocimetry (PIV) technique. This study yielded data on the Mach disk geometry and velocity profiles downstream from the Mach disk. In the second campaign, thermal conditions of the hot jet impact on a metal plate were investigated by measuring the temperature field on the plate back. The temperature measurements were performed with an infrared camera.

2. Experimental facility for hot jet generation

Studied jets were created by a hot-gas generator, which can be viewed as a cylindrical combustion chamber with a sonic throat at its outlet. The throat diameter is D_j = 25 mm A schematic view of the hot-gas generator with main dimensions and supplying lines is presented in Fig. 1.

The combustion chamber is fed with air and liquid kerosene at normal temperature. The two fluids are input separately through several injection orifices near the upstream end of the chamber. At startup, the combustible mixture is ignited by a flame torch injected into the chamber. The pressure and temperature in the combustion chamber are controlled as functions of the total mass flow rate G_j and fuel equivalence ratio ϕ.

The combustion chamber is made of stainless steel. The internal walls of the chamber are water-cooled allowing continuous operation. Thus, the test run duration is only limited by the air storage capacity, which is sufficient to supply a mass flow rate about 1.5 kg/s during several minutes.

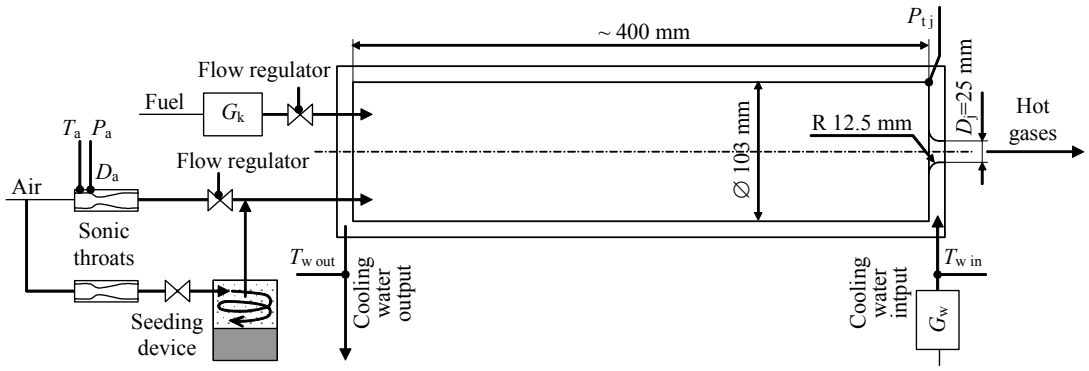

Figure 1: Scheme of the hot-gas generator with supplying lines.

To characterize the operation regime, the following measurements are performed:
– flow rate of main air is determined using a calibrated sonic throat; another sonic throat is in a secondary line for the flow seeding, which is described in the next section;
– flow rate of kerosene is measured by a flowmeter;
– pressure in the combustion chamber is measured on the wall close to its downstream end; the measured pressure is considered equal to the total pressure, P_{tj}, of jet ejection because the flow velocity is low in the combustion chamber;
– flow rate of cooling water and temperature difference at the water output and input to evaluate the heat losses to the cooling system.
There are no means to directly measure the gas temperature at the chamber outlet. Instead, an integral method, based on the global mass and energy balances inside the hot-gas generator, is employed for the total temperature evaluation. Assuming a unity Mach number and equilibrium composition at the combustion chamber exit, the total temperature, T_{tj}, must satisfy the two balance conditions. To make it possible, the combustion efficiency is introduced in the thermodynamic relations providing that some fraction of the injected fuel may not react.
A series of qualification tests has been performed to evaluate the thermal state of the hot-gas flow. It was verified that the combustion efficiency is greater than 0.96. Taking into account the combustion efficiency and heat losses due to the wall cooling, the mean difference between the ideal combustion temperature and the average total temperature, T_{tj}, is about 150 K for T_{tj} = 1600-2200 K.

2. PIV measurements of velocity field

PIV technique is a powerful method as it allows obtaining accurate measurements of instantaneous and mean velocity field in a plane. Being widely applied to subsonic flows, PIV has been used as well to measure velocity fields in supersonic flows[1,2,3,4]. In a supersonic flow, velocity variations can be very rapid especially across shock waves. Hence, flow tracking is an important problem because it is necessary to provide a short response time of flow seeding particles[5]. For a hot flow, seeding particles must be temperature-resistant so the problem of flow seeding is even more complicated. A relatively small number of studies has been made on hot-gas supersonic flows. Conditions obtained in the experiments of Goyne et al.[6] and Weisgerber et al.[7] are comparable to those corresponding to the present study.

2.1 PIV system

The layout of the PIV system employed in the present study is shown in Fig. 2. Particle visualization is made in the vertical plane passing through the jet axis. A twin-head 532 nm Nd-Yag laser, Quantel Ultra PIV 120, is used as a light source. It can generate pulses of collinear laser beams by pairs with a controlled pulse separation time. The nominal pulse energy is of 120 mJ and the pulse duration is of 12 ns.
An optical system consisting of a mirror and two lenses is mounted on a common support with the laser. The mirror redirects the laser beams vertically through the jet axis. A convergent spherical lens, f = 592 mm, helps to focus the laser beams on the level of the jet. Then, a plano-cylindrical lens, f = –12.7 mm, expands the beams along the jet axis thus creating two superimposed laser sheets. The laser plane has a width of 270 mm and a mean thickness of approximately 0.6 mm within the measurement zone.
Particle images are detected by a CCD camera, TSI Powerview 2M, with a number of pixels of 1200 × 1600 and a sensor dynamics of 10 bits (1024 grey levels). The minimal time separation between the two frames of an image pair is of 0.2 μs. The acquisition frequency of image pairs has been set at 15 Hz, the maximum rate allowed by the laser

system. The camera is placed at 90° with respect to the laser plane at a distance of approximately 800 mm (see Fig. 2). An Nikon objective, f = 50 mm, provides the desired magnification of the observation zone 208 mm × 156 mm with a spatial resolution of 130 µm/pixel.
Image acquisition and laser pulses are controlled by a synchronizer, TSI Laser Pulse. The time interval Δt between two laser pulses was set from 0.4 µs to 1 µs according to the flow velocities estimated or measured from the previous experiments. The total duration of image series acquisition was of 10 s. During this period, the jet conditions were sufficiently stable (variation of ejection conditions less than 1 %) to allow computing the mean velocity field from the whole image series.

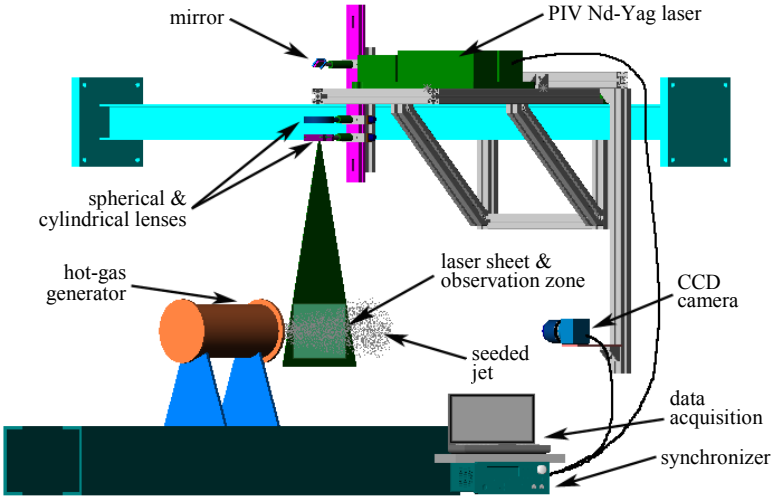

Figure 2: Schematic of the PIV implementation.

2.2 Flow seeding

In this study, solid particles of SiO_2 (commercial designation “Aerosil R812”) were used for seeding because of the following main requirements: high temperature resistance and the lowest possible particle size. The latter requirement ensures the flow tracking at a very high speed[7]. Particles have the following main properties: mean diameter of primary particle of 7 nm, melting point of 1970 K, density of 2000 kg/m^3. In spite of the fact that particles could be melted in the hot flow, no significant particle deposits were found on the combustion chamber walls. A specific test was made using Al_2O_3 particles to validate SiO_2 seeding.
Seeding particles are introduced into the main air line next to the hot-gas generator (see Fig. 1). To do this, a secondary air flow is passed through a seeding device, whose operation is based on the principle of cyclone: the air is injected tangentially at a high speed into a cylindrical reservoir containing particles; the swirl motion creates a depression in the center and entrains particles from the bottom; air seeded with particles is drawn from the top of the central zone.
The ability of seeding particles to follow the fluid motion is of fundamental importance when PIV is applied to a supersonic flow. As the particles have a finite mass, they are unable to respond instantaneously to the flow velocity variation. Following Melling[5], one can apply the Stokes law to evaluate the particle response time τ_S, during which the velocity difference due to the particle slip is reduced by a factor of e. Based on manufacturer’s specification of individual particle properties, τ_S is unrealistically low, of the order of 0.1 µs. Nanometric particles have a tendency to form agglomerates whose properties, i.e. mean diameter and density, can be significantly different from those of the primary particle. The common practice is to deduce the effective particle diameter by fitting the solution of the Stokes equation to the experimentally observed slip behind a choc. In the present study, the particle slip becomes indistinguishable at about 5 mm behind the Mach disk. The corresponding time constant τ_S is 1.5 µs. Taking the density of particle material, the effective particle diameter is of 0.62 µm. These figures agree with the values commonly found in literature[2]. In the present study, SiO_2 particles are preferred to Al_2O_3 particles thanks to a lower density and hydrophobic properties that reduce the particle agglomeration.

2.3 PIV results

In the test series with PIV measurements, the stagnation conditions at the exit of the hot-gas generator varied within the following ranges: P_{tj} = 2.65-3.84 MPa, T_{tj} = 1770-2140 K. PIV measurements were conducted for two zones identified by the axial distance from the jet ejection section: x = 5-205 mm and 123-323 mm. The main objective was to investigate the velocity field within the second zone (x = 123-323 mm) where the conditions are the most suitable for the PIV method. Most of the data were obtained within that zone. Because of seeding difficulties in the first zone, measurements were made to characterize the Mach disk geometry and to check the applicability limits of the measurement system.
Besides quantitative measurements of the velocity field, PIV images provide useful information on the jet. Figure 3 presents a combination of instantaneous images from the two measurement zones to visualize the jet structure. The expansion of ejected gases rapidly accelerates the jet flow making it supersonic. Diverging streamlines are clearly visible within the expansion region on the left side of the image. The expansion is so strong that the static pressure falls below the ambient pressure level. A so-called barrel shock equilibrates the flow pressure with the ambient pressure around the jet. Past the barrel shock, the jet flow remains supersonic. A strong shear between the jet flow and ambient air produces a turbulent layer along the jet boundary. In the central region, the supersonic flow passes through a normal shock, or a Mach disk. Behind the Mach disk, the pressure is somewhat higher than past the barrel shock, thus a reflected shock appears at the junction of the barrel shock and Mach disk. Behind the Mach disk, there is a large subsonic zone that contracts as the surrounding supersonic flow forms a kind of throat. Large-scale turbulent structures develop around this subsonic zone and occupy entirely the jet past the throat.

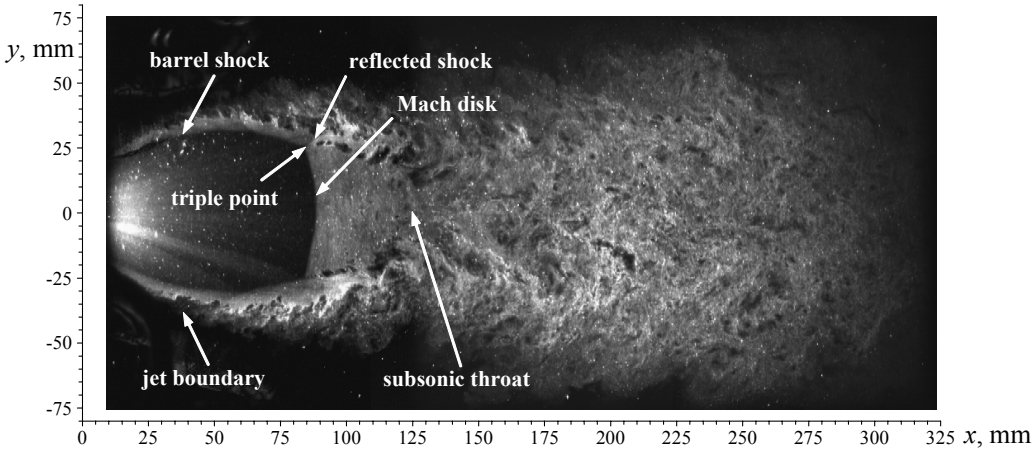

Figure 3: Jet structure visualized by instantaneous PIV images from the two measurement zones. Jet ejection section is beyond the left edge of the image. Jet stagnation conditions: P_{tj} = 2.68 MPa, T_{tj} = 1970 K.

Direct processing of instantaneous PIV images permitted us to measure the Mach disk geometry. The axial position of the Mach disk and the triple point coordinates obtained from the instantaneous images have been averaged to evaluate the Mach disk diameter D_{MD} and the distances from the jet ejection section to the Mach disk center L_C and to the triple point L_{TP}. The results on L_C agree with the correlation proposed by Crist et al.[8], which can be expressed as $L_C/D_j = 0.645\ (P_{tj}/P_a)^{0.5}$, where P_a is the ambient pressure. Using this kind of fit, the results of the present study can be approximated as follows: $D_{MD}/D_j = 0.4138\ (P_{tj}/P_a)^{0.5}$, $L_C/D_j = 0.6861\ (P_{tj}/P_a)^{0.5}$, $L_{TP}/D_j = 0.6517\ (P_{tj}/P_a)^{0.5}$. One can observe that the Mach disk has a slightly convex shape ($L_C > L_{TP}$).
To determine the velocity field, the PIV images were analyzed after the experiment by a cross-correlation algorithm using the TSI Insight 6.0 software. The interrogation window size in pixels was 32 × 32 with a 50 % overlap shifting. The optical calibration factor was determined as 130 μm/pixel, thus the maximum particle displacement of about 11 pixels could be expected for a velocity of 1500 m/s and a laser pulse separation time of 1 μs.
A post-treatment was done on the instantaneous vector fields. A standard deviation filter was applied to remove spurious velocity vectors produced by poor correlation at some points. The number of vectors rejected by this filtering was below 100 vectors by image (< 2 %) for the zone x = 123-323 mm. For the zone x = 5–120 mm, the number of rejected vectors was largely higher, especially in front of the Mach disk where it exceeded 50 %. This is due to nonuniform seeding quality over the image (see Fig. 3). The seeding was adjusted to provide a good particle density downstream from the Mach disk without image saturation, but it was insufficient in front of it. This is due to the fact that the velocity ratio before and after the Mach disk is about 5, and the change in seeding density is directly

proportional to this factor. Measurement points with low signal-to-noise ratio are rejected by the filter, thus poorly seeded PIV recordings return only a few velocity vectors. Only visible large particles (agglomerates) provide information for the correlation procedure but these particles are not good flow tracers. Thus the flow velocity measurement in front of the Mach disk is subject to two important problems: poor correlation and large particle slip.
For the conditions of the present study, it has been found that the velocity field downstream from the Mach disk is almost independent of the jet total temperature. In Fig. 4, several axial distributions of velocity magnitude, u, corresponding to a nearly constant total pressure $P_{tj} \approx 3.2$ MPa and largely variable total temperature $T_{tj} = 1830$-2140 K, are put together. The axial velocity distributions are quasi-insensitive to the variation of T_{tj}. This observation is also confirmed by the comparison of radial profiles of u presented in Fig. 5 for $P_{tj} \approx 2.7$ MPa and the same range of T_{tj}. This quasi-independence of the velocity field from T_{tj} has the following explanation: the properties of the combustion products are conditioned by the total temperature as it is in direct relation with the quantity of burnt fuel; in particular, the specific heat ratio of combustion products is affected by the temperature and gas composition in a manner that the sound speed is not very different over the explored range of total temperature variation. From numerical simulations, it has been found that the velocity differences are important at a high Mach number in front of the Mach disk. Unfortunately it was not possible to accurately measure the flow velocity in that zone.

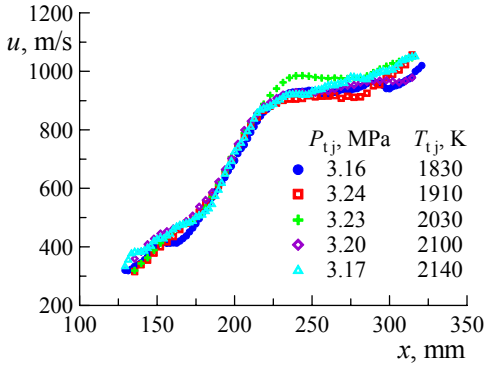

Figure 4: Axial distributions of velocity magnitude for constant P_{tj} and variable T_{tj}.

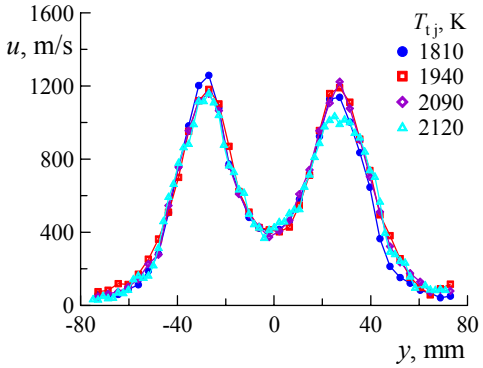

Figure 5: Radial profiles of velocity magnitude for constant $P_{tj} \approx 2.7$ MPa and variable T_{tj}, $x = 135$ mm.

On the other hand, an important effect of the jet total pressure on the studied velocity field has been identified. Nevertheless, a clear similarity can be found between the velocity fields if one uses non-dimensional coordinates $(x - L_C)/D_{MD}$ and y/D_{MD}. This similarity is demonstrated in Fig. 6 by longitudinal distributions of u and in Fig. 7 by radial profiles of u. The results are taken for the range of P_{tj} from 2.67 MPa to 3.67 MPa and a small variation of T_{tj} around 1840 K. To compare the radial profiles in Fig. 7, the sections $x = 135$ mm and 175 mm for $P_{tj} = 2.67$ MPa correspond to the same values of similarity coordinate $(x - L_C)/D_{MD}$ as the sections $x = 158$ mm and 206 mm for $P_{tj} = 3.67$ MPa. The present analysis suggests that the Mach disk diameter D_{MD} and distance L_C are characteristic geometric parameters of the studied jets.

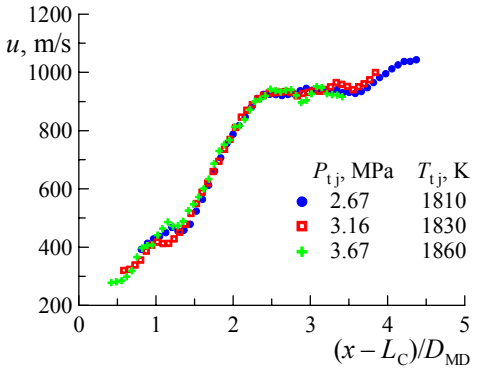

Figure 6: Axial distributions of velocity magnitude for variable P_{tj} and constant T_{tj}.

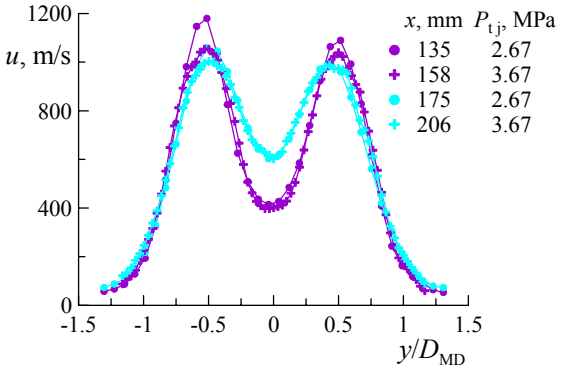

Figure 7: Radial profiles of velocity magnitude for variable P_{tj} and constant T_{tj}.

3. Infrared temperature measurements on a metal plate

Thermal conditions of the hot jet impact on a metal plate have been studied using an infrared camera. The temperature measurements have been performed on the back of a titanium plate 400 mm × 400 mm × 10 mm. From the temporal evolution of the temperature field on the back side, it is possible to reconstruct heat fluxes on the front side by solving an inverse thermal problem[9].

3.1 Experimental setup for infrared measurements

The experimental setup is schematically shown in Fig. 8. A tested plate is installed normally to the jet axis at a distance of 350 mm from the exit of the hot-gas generator. The plate is thermally isolated from its support. An infrared camera, ThermaCAM SC3000, with a 12º objective is set in a housing, which is intended to protect the camera from the hot flow. An Al-coated optical mirror 200 mm × 200 mm is used as an additional protective measure to dispose the camera away from the direction of impact.
A pivoted shield controlled by a pneumatic actuator is installed between the hot-gas generator and the tested plate. During the combustion chamber startup, the jet impinges on the shield and is turned upwards to prevent its contact with the plate. When the specified jet conditions are reached, the shield is instantly removed.

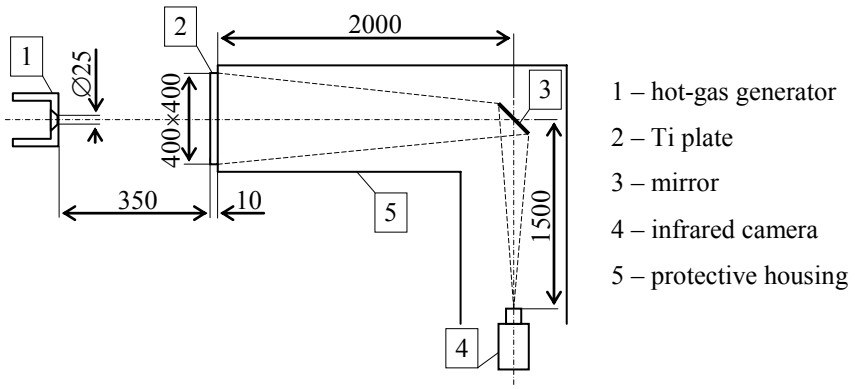

Figure 8: Experimental setup for infrared measurements. All dimensions in mm.

Infrared measurements require that the object emissivity is sufficiently high, to provide a strong signal, and stable, to guarantee precise temperature measurements over the whole temperature range. On the contrary, metals have weak emissivity, which can change during heating due to the oxidation. To enable infrared measurements, a 40±6 μm layer of Al_2O_3 ceramics is deposited on the plate back by plasma coating. Al_2O_3 ceramics is known to have a high and stable emissivity at wavelengths 8-9 μm corresponding to the operation range of SC3000.

3.2 Experimental results

This section presents experimental results obtained for the following jet conditions: P_{tj} = 3.5 MPa, T_{tj} = 1930 K and 2080 K. The duration of jet impact was 3 min. Every test was made with a new plate.
The following parameters were specified for the image acquisition: frame rate of 10 Hz, temperature range ≤ 2000ºC. Image series were recorded during the tests and then analyzed using the ThermaCAM Researcher 2001 software. Wall temperature was determined for an emissivity of 0.99 and an external optics transmission of 0.975. The wall emissivity was measured by infrared spectroscopy on specific samples. The external optics transmission characterizes the mirror reflectivity, which was experimentally determined using the same infrared camera. Spatial resolution of the infrared images is 1.667 mm per pixel.
Photographic images of a plate after the test are presented in Fig. 9. The front is significantly oxidized whereas the back is absolutely intact thanks to the ceramic coating. An important deformation is caused by the hot-jet impact. After the first test (T_{tj} = 1930 K) the deformed zone has a diameter of 310±5 mm and a depth of 18 mm whereas, after the second test (T_{tj} = 2080 K) the deformation dimensions are respectively 327±5 mm and 24 mm.

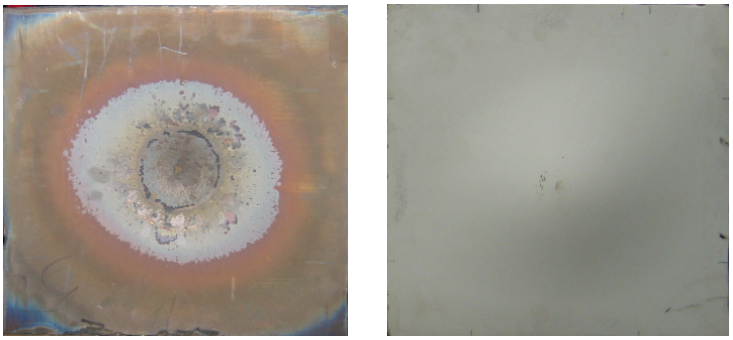

Figure 9: Front (on the left) and back (on the right) sides of a plate after the test.

Several instantaneous infrared images are presented in Fig. 10 demonstrating the wall temperature evolution during the first test. The last image shown corresponds to the time moment when the maximum wall temperature reached its upper limit at about 1120ºC. The minimum temperature indicated on the images corresponds to the lower limit of the measurement range.

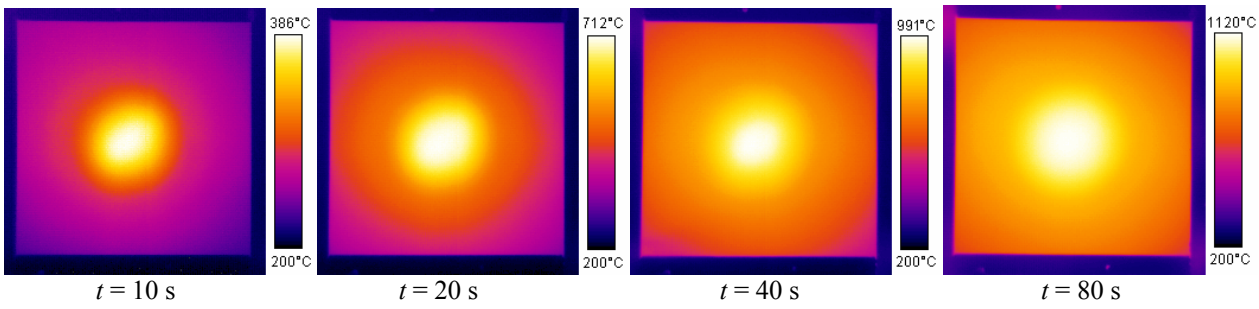

Figure 10: Infrared images of the plate back for T_{tj} = 1930 K.

Measured temporal evolution of the maximum temperature, $T_{b\,max}$, is plotted in Fig. 11 for the two tests. Upper temperature limits of 1118±8ºC and 1185±10ºC are obtained almost at the same time $t \approx 72$ s. A singular point is observed at $T_{b\,max} \approx 900$ºC, at which the temperature slope abruptly increases. This behavior can be explained by the transition of the Ti crystalline structure from the hexagonal (alpha) form into the cubic (beta) form that normally takes place at 882ºC[10]. Before the transformation, the heat conductivity strongly increases, and with the transformation, it reduces and then remains constant.

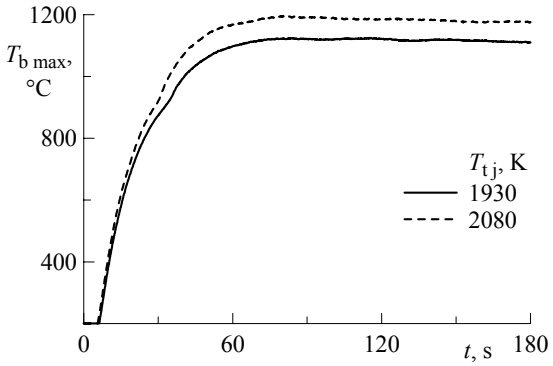

Figure 11: Temporal evolution of the maximum temperature on the plate back.

Temporal evolution of the temperature distribution on the horizontal symmetry axis is shown in Fig. 12 for the two tests. One can notice that the distribution of T_b is slightly shifted to the left from the vertical axis (z = 0). After 100-120 s of jet impact, the thermal state of the plate is stabilized in the central zone (–0.1 m < z < 0.1 m). Close to the plate edges (z = ±0.16 m), T_b increases by 10ºC with respect to its mean value of 850-900ºC during the last 20 s.

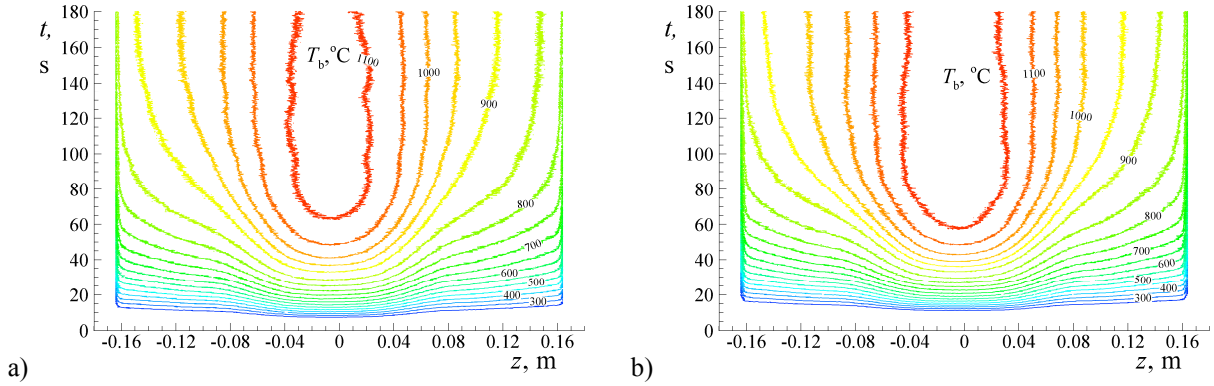

Figure 12: Temporal evolution of the temperature distribution on the horizontal symmetry axis for T_{tj} = 1930 K (a) and T_{tj} = 2080 K (b).

4. Conclusion

Experimental studies of underexpanded hot-gas jet have been performed to provide data on the velocity field in a free jet and characterize thermal state of a titanium plate during a hot-jet impact. These data can be used for the validation of numerical tools applied to studies on the aircraft engine safety.

Acknowledgments

The authors thank Dr. Patrick Echegut from CRMHT-CNRS in Orléans for his help in determining the emissivity of ceramic coatings.

References

[1] Humphreys, W. M., Bartram, S. M., and Blackshire, J. L. A Survey of Particle Image Velocimetry in Langley Aerospace Facilities. AIAA Paper 93-0411, 1993.

[2] Urban, W. D. and Mungal, M. G. Planar velocity measurements in compressible mixing layers, *Journal of Fluid Mechanics*, 431:189-222, 2001.

[3] Scarano, F. and van Oudheusden, B. W. Planar velocity measurements of a two-dimensional compressible wake, *Experiments in Fluids* 34:430-441, 2003.

[4] Schrijer, F. F. J., Scarano. F., and van Oudheusden B. W. Application of PIV in a Mach 7 double-ramp flow, *Experiments in Fluids*, 41:353-363, 2006.

[5] Melling, A. Tracer particles and seeding for particle image velocimetry, *Measurement Science and Technology*, 8:1406-1416, 1997.

[6] Goyne, C. P., McDaniel, J. C., Krauss, R. H., and Day, S. W. Velocity measurement in a dual-mode supersonic combustor using particle image velocimetry, AIAA-2001-1761, *10th AIAA/NAL-NASDA-ISAS Space Planes and Hypersonic Systems and Technologies Conference*, Kyoto, Japan, 24-27 April 2001.

[7] Weisgerber, H., Martinuzzi, R., Brummund, U., and Magre, Ph. PIV measurements in a Mach 2 hydrogen-air supersonic combustion, AIAA-2001-1757, *10th AIAA/NAL-NASDA-ISAS Space Planes and Hypersonic Systems and Technologies Conference*, Kyoto, Japan, 24-27 April 2001.

[8] Crist, S., Sherman, P. M., and Glass, D. R. Study of the highly underexpanded sonic jets, AIAA Journal, 4(1):68-71, 1966.

[9] Reulet, P., Nortershauser, D., and Millan, P. Inverse method using infrared thermography for surface temperature and heat flux measurements, *ICIASF '03 20th International Congress on Instrumentation in Aerospace Simulation Facilities*, Göttingen, Germany, 25-29 August 2003.

[10] Titanium, in: Wikipedia, the free encyclopedia, URL: http://en.wikipedia.org/wiki/Titanium#_note-EncyChem

This page has been purposedly left blank